Publishing House
AKAPIT

COMPUTER METHODS IN MATERIALS SCIENCE

Informatyka w Technologii Materiałów

Vol. 15, 2015, No. 1

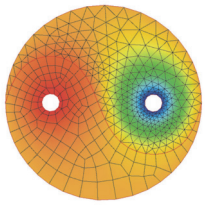

THE NUMERICAL ANALYSIS OF A TITANIUM SHEETS WELDING PROCESS AND WELDING JOINT TENSILE BEHAVIOR

KONRAD ADAMUS*, PIOTR LACKI

Częstochowa University of Technology, ul. Akademicka 3, 42 200 Częstochowa, Poland
**Corresponding author: konrad.adamus@gmail.com*

Abstract

The paper analyses joining of titanium Grade 2 and Grade 5 sheets using electron beam welding, EBW, technology. The joined sheets undergo further processing to produce final aircraft component.

EBW is a fusion welding process that utilizes electrons to produces heat and join materials. It is characterized by low heat input, small distortions, precise and repeatable welding parameters and vacuum operating conditions. Titanium is a unique material that offers high specific strength, heat resistance and corrosion resistance. In aerospace applications it is used for components of rotors, engines and airframes. Tailor Welding Blanks is a technology of joining sheets of different properties in order to obtain components that have mixed properties. Titanium Grade 2 has better formability while titanium Grade 5 has higher strength. The welded sheets are further formed in order to obtain final shape.

The numerical simulation of the welding process investigates the impact of thermal load produced by a moving electron beam on the deformations occurring in the joined sheets. The model is based on finite element method and it takes into account elastic, plastic and thermal strains. The analyzed sheets have thickness of 0.8 mm, their small cross-section contributes to significant post-welding bending both in transverse and longitudinal directions. The paper analyzes the influence of mesh structure and welding gap on the degree of deformation. The obtained numerical results were compared with actual welding deformations. The research into modeling of titanium sheets welding was extended with analysis of joint behavior during tensile tests. Specimen was cut out from the joint and was subject to uniaxial tensile test. The strains occurring during tension were recorded using optical non contact measurement system that uses two cameras. The experimentally measured strains were compared with numerical results from a separate finite element method model.

Key words: electron beam welding, welding distortions, welding gap, thin sheets, finite element method

1. INTRODUCTION

In the work a finite element method model of thin sheets electron beam welding was presented. The problem of welding thin sheets was selected as it produces high distortions in the material and can validate the welding model's accuracy. According to Lindgren (2007) accurate predicting of post-welding deformations is more difficult than predicting residual stresses. A number of factors impact on calculated deformations and residual stresses, among others: welding gap, mesh structure and weld bead geometry.

Interface elements can be used for modeling of welding gap between sheets (Wang et al., 2013; Murakawa et al., 2012; Deng et al., 2012). Interface element technique consist in applying nonlinear spring elements joining the welded sheets. The definition of relationship between displacement and bonding force allows for taking into account bonding strength, gaps and misalignments occurring at different stages of a welding process.

Moein and Sattari-Far (2014) investigated the application of different element techniques to modelling of a welding gap and their impact on magnitude of calculated residual stresses in a simulation of

ISSN 1641-8581

aluminum welding process. Three cases were analyzed: welded sheets were simulated as a single block of material, birth element option was used to represent moving welding pool, interaction technique was used to describe the surface-to-surface thermal and structural contact between welded sheets. The study showed that element birth technique yielded most accurate results for residual stresses. Arai (2010) analyzed the case of welding thin sheets fixed with clamping device and noted that there are significant discrepancies in calculated deformations between models taking into account and not taking into account a welding gap. Shan et al. (2007) compared element birth technique with sheets as single block technique. It was found out that element birth technique produces more accurate temperature field. Koch et al. (2013) modelled welding of curved plates. One of the plates was at the top of the another. In order to simulate the air gap between the overlapping plates the conductive and radiative heat exchange between the gap surfaces was taken into account.

2. EXPERIMENT

During experimental research two titanium sheets of different grades were joined using electron beam welding, EBW, technology. EBW is a fusion welding technology that utilizes a beam of electrons to melt metals which after crystallization form a joint. Extensive description of EBW can be found in (Schultz, 2000). During welding the sheets were fixed using a clamping device. Both sheets had the same dimensions: 0.8 x 130 x 125 mm.

One of the sheets was made of titanium Grade 2 that is characterized by good formability and the other from titanium Grade 5 that is characterized by high strength. The purpose of joining titanium sheets of different grades is to produce Tailor Welded Blanks, TWB, that will undergo further forming operations to produce final aircraft component. Application of titanium to TWB was described in (Winowiecka et al., 2013; Adamus & Lacki, 2014).

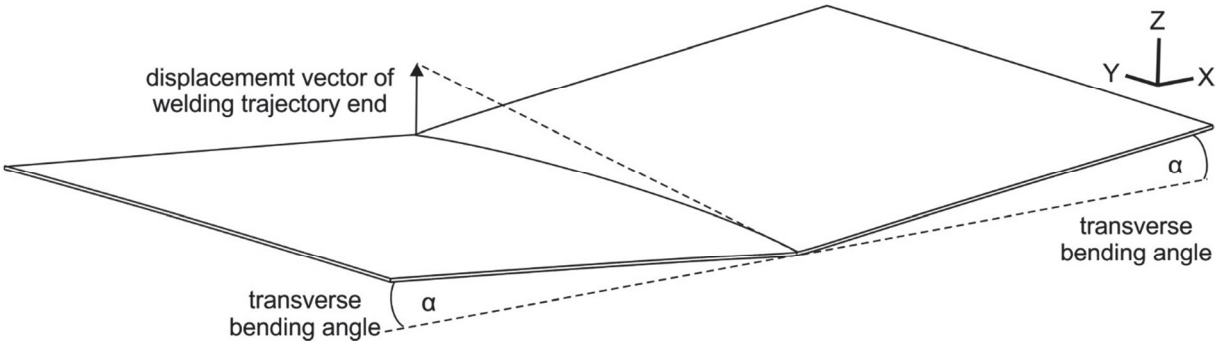

Fig. 1. *The measures of deformation: the bending angle α for transverse bending, the displacement vector of the end of a welding trajectory for longitudinal bending.*

Schenk et al. (2009) analyzed the dependency of distortion amplitude on finite element mesh for welding simulations. The authors showed that adequate prediction of distortions requires fine mesh resolution everywhere where bending occurs and it is not enough to use high element densities only where high stress and temperature gradients occur. Two kinds of mesh were investigated: coarsening towards sheet sides (T-meshes) and non coarsening towards sheets sides (L-meshes). T-meshes don't produce acceptable results and the best results were obtained for L-meshes.

According to (Sun et al., 2014; Matsuoka et al., 2013) accurate description of the heat source is essential to the simulation of thin-sheet welded structures and has significant impact on the final deformation of thin sheets.

The welding process introduces deformations into the sheets: transverse bending and longitudinal bending. Figure 1 presents the character of sheet distortions and distortions measures. Transverse bending is measured by butterfly angle α, longitudinal bending is measured by displacement vector of the end of a welding trajectory.

3. THEORY AND CALCULATIONS

Computational welding mechanics models usually fall into one of the two categories: computational fluid mechanics, CFD, or computational solid mechanics, CSM. CFD models describe fluid motion inside weld pool and aim at predicting fusion zone, FZ, shape based on welding parameters (Piekarska et al., 2010; Słoma et al., 2011). CSM models pre-

dict stresses and displacements occurring as a result of thermal load (Lacki et al., 2014).

This study uses CSM model to describe deformations of the welded sheets. Thermo-mechanical coupled analysis was applied. The model was built using ADINA program. Finite element procedures used in ADINA can be found in (Bathe, 2006).

Transient heat transfer was described by Fourier-Kirchoff equation:

$$\frac{\partial T}{\partial t} = a\nabla^2 \mathrm{T} + \frac{q_v}{\rho c_p} \qquad (1)$$

where: a – the thermal diffusivity, ρ – the density, c_p – the specific heat, q_v – the efficiency of internal volume heat source.

The equation defining thermo-elasto-plastic material has the following form:

$${}^{t}\sigma_{ij} = {}^{t}C^{E}_{ijrs}({}^{t}e_{rs} - {}^{t}e^{P}_{rs} - {}^{t}e^{TH}_{rs}) \qquad (2)$$

where: ${}^{t}\sigma_{ij}$ – stress tensor at time t, ${}^{t}C^{E}_{ijrs}$ – elasticity tensor at temperature corresponding to time t, ${}^{t}e_{rs}$ – total strain tensor at time t, ${}^{t}e^{P}_{rs}$ – time independent plastic strain tensor at time t, ${}^{t}e^{TH}_{rs}$ – thermal strain tensor at time t.

Plastic strains were calculated using von Mises model with isotropic hardening. Thermal strains were calculated based on temperatures in nodes and thermal expansion coefficient. Relationship between stresses and strains was described using bilinear model. The computational model takes into account dependency of physical properties on temperature. The detailed information about applied values of material properties can be found in (Adamus et al., 2013).

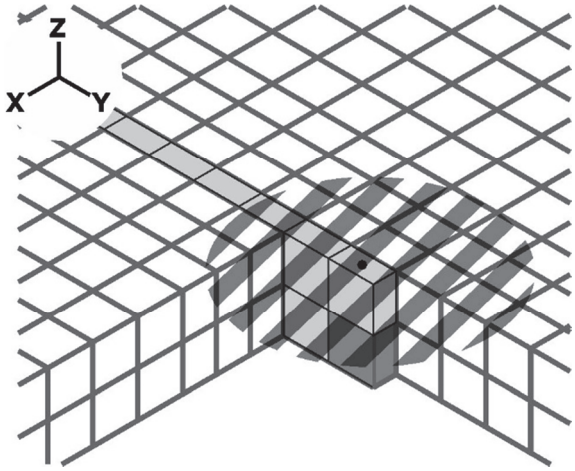

Fig. 2. *The fragment of mesh representing sheets (white elements) and welding gap (gray elements). Surface disk heat source was denoted with striped pattern. Volumetric heat source was denoted with dark gray, underneath disk.*

The welding model uses combined surface and volumetric heat source model. The outline of the heat source is presented in figure 2.

White elements denote sheets and light gray elements denote the volume of material that is filling the initial welding gap. For clarity, the part of mesh corresponding to the sheet in direction of positive values on X axis was removed. The black dot denotes the current position of the heat source. As the heat source moves along the welding trajectory (Y axis) the consecutive elements fill the gap between sheets. The occurrence of the welding gap elements is implemented using element birth option. If this options is set elements will become present in the simulation after simulation time exceeds their birth time. Surface heat source in the shape of a disk was denoted with striped pattern. Below the disk heat source there is volumetric heat source consisting of a single element denoted with dark gray color. Both heat sources move together, along the welding trajectory, with step equal to the length of element edge in Y axis direction. During calculation 90% of power was assigned to the surface heat source and 10% of power was assigned to volumetric heat source.

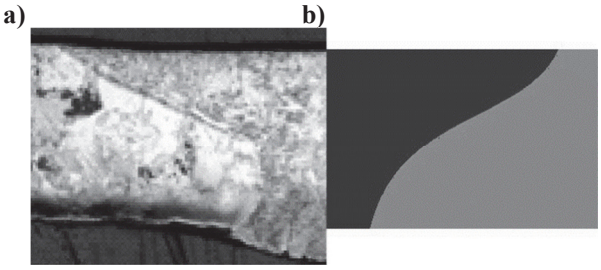

Fig. 3. *The comparison of the FZ geometry: actual (a) and calculated (b).*

Figure 3 presents the comparison of FZ calculated by the welding model and the macrostructure of the actual FZ. The macrostructure of the specimen cross-section shows that even though the sheet has small thickness, there is significant change of FZ geometry with increasing depth.

Figure 4a presents the outline of the welding model geometry. Gray planes show the interface between welded sheets and clamping device. The clamping device was modeled using spring elements with high stiffness attached to appropriate nodes. Figures 4b and 4c present fragments of mesh structures used in the study.

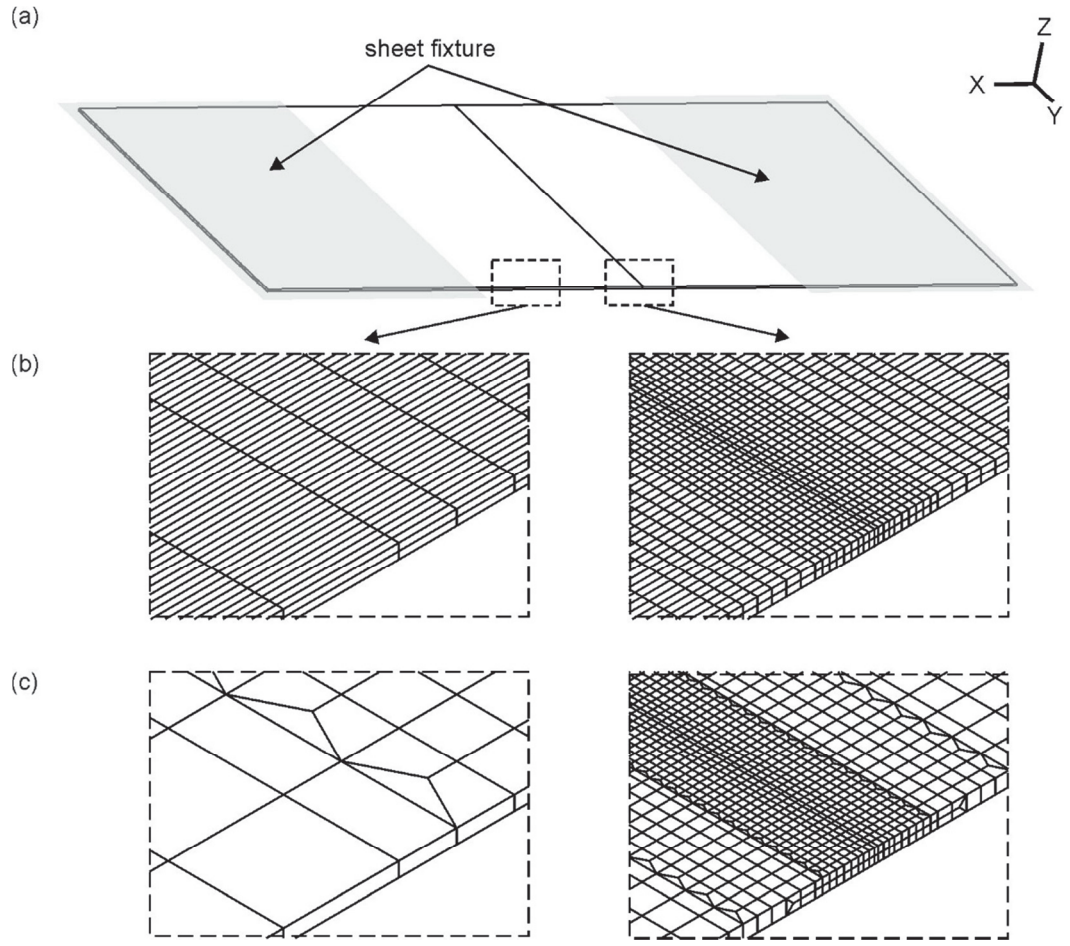

Fig. 4. *Welded sheets: geometry (gray planes denote fixture holding sheets during welding) (a), mesh with no reduction along Y and Z axes (b), mesh with reduction along Y and Z axes (c).*

During research 5 different models were analyzed:

- Model A: the number of elements in direction of Z and Y axes was constant, figure 4b. Element birth option was used to simulate initial welding gap.
- Model B: the number of elements in direction of Y axis was decreasing and in direction of Z axis was constant. Element birth option was used to simulate initial welding gap.
- Model C: the number of elements in direction of Y axis was constant and in direction of Z axis was decreasing. Element birth option was used to simulate initial welding gap.
- Model D: the number of elements in direction of Y and Z axes was decreasing, figure 4c. Element birth option was used to simulate initial welding gap.
- Model E: the number of elements in direction of Z and Y axes was constant, figure 4b. There was no initial welding gap and sheets were treated as single block of material.

4. RESULTS

Table 1 presents the summary of calculated deformations for model A-E. A discrepancy is defined as:

$$d = (v_c\text{-}v_a)/v_a \tag{3}$$

where: v_a - actual value, v_c - calculated value. It can be seen that best results were obtained for model A that has constant number of elements in directions of Y and Z axes and utilizes element birth option to represent initial welding gap. The reduction of the element count in Y direction causes significant increase in the discrepancy of longitudinal bending, from 18 to 50 %. The reduction of the element count in Z direction increases the discrepancy of longitudinal bending to a lower extent, from 18 to 30 %. For models A-D the worst results were obtained for model reducing element count in Y and Z directions. The analysis of results obtained for model E, which has the same mesh as model A, shows that the lack of initial gap in the welding model contributes to the greater discrepancy than the reduction of mesh density, both for transverse and longitudinal bending.

Table 1. *The discrepancy between actual and calculated bending for different mesh structures.*

Welding model	Transverse bending discrepancy, %	Longitudinal bending discrepancy, %
A no mesh reduction along Y and Z axes, element birth	-18.5	-23.7
B mesh reduction along Y axis, element birth	-18.7	-50.4
C mesh reduction along Z axis, element birth	-17.7	-29.2
D mesh reduction along Y and Z axes, element birth	-24.3	-53.0
E no mesh reduction along Y and Z axes, sheets as single block of material	-77.7	-57.7

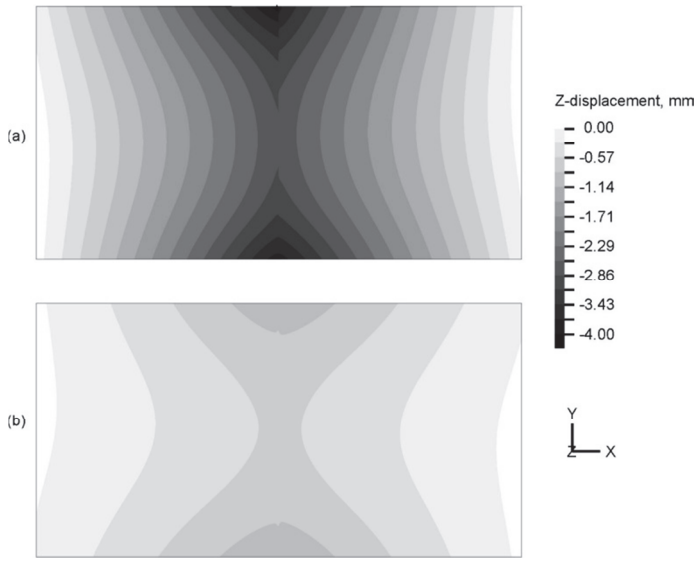

Fig. 1. *Z-displacement distribution: model with initial welding gap, variant A (a), model without initial welding gap, variant E (b).*

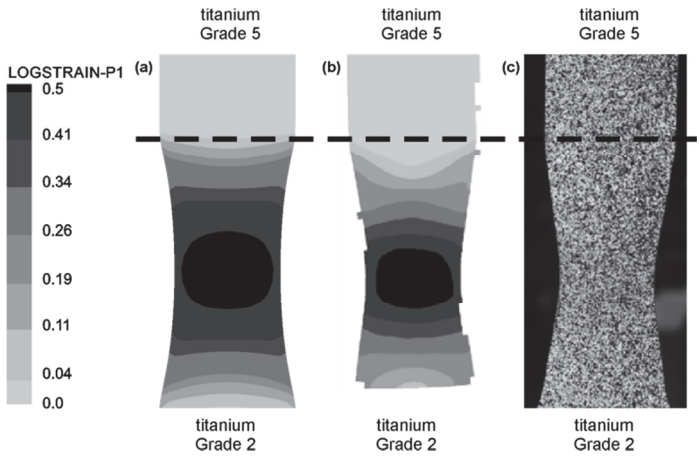

Fig. 2. *Logarithmic principal strain distribution during uniaxial tensile test: numerical results (a), experimental measurements (b). Stochastic pattern used for experimental measurements (c). The dashed line denotes the position of the welding line.*

Figure 5 presents the distribution of displacement along Z axis i.e. in the direction of sheet thickness. Z-displacement equal to 0 corresponds to the initial position of the sheet top surfaces. Part (a) corresponds to model A that takes into account the initial welding gap, part (b) corresponds to model E that treats sheets as single block of material. The character of deformation in both cases is similar. There is convex longitudinal bending and concave transverse bending. However, there is large difference in the minimal value of Z-displacement, about 4.1 mm for model A and about 0.8 mm for model E. For model A there is distinct shift in the displacement values along welding trajectory. The shift occurs to a smaller extent also for model E. In case of model E the shift corresponds to slightly concave weld face. In case of model A the additional factor is the difference in displacement between Grade 2 and Grade 5 sheet edges. The shift increases toward the end of the welding trajectory, corresponding to higher Y axis values. The shift occurred also in the actual welded sheets, as difference between sheet edges near the welding trajectory end was about 25% of the sheet thickness.

Figure 5 presents the distribution of logarithmic principal strain during uniaxial tensile tests in specimen cut out from welded sheets. The specimen in the shape of a strip was cut out in the direction perpendicular to the welding trajectory. Part (a) corresponds to results obtained from numerical model. During calculations the same material model was applied as in case of the welding simulation. Part (b) corresponds to experimental measurements at time before the onset of the crack. The measurements were performed using optical system Aramis. The system uses two cameras to track the motion of stochastic pattern, in the form of black dots with white background, spray painted at the sheets' external surface, figure 6c. During numerical calculations of uniaxial tension necking occurred in the specimen at the side of titanium Grade 2 sheets, which has lower strength. The strains at the side of titanium Grade 5 were minimal. In the case of experimental measurements the necking also occurred at the side of titanium

Grade 2 sheet. There is similarity between the strain fields calculated by the numerical model and measured by the optical system.

5. CONCLUSIONS

In the work thermo-mechanical model of thin sheets welding process was described. The goal of the model was to predict deformations occurring due to the welding process. Different finite element meshes and welding gap models were analyzed. Based on the performed analysis the following conclusions can be drawn:

- Computational welding models predicting distortions of thin sheets are very sensitive to mesh structure and welding gap model.
- The best results with regard to accuracy of transverse and longitudinal bending prediction were achieved for meshes that avoid reduction of element count in directions corresponding to sheet thickness and welding trajectory, in the volume of sheets away from welding line.
- The discrepancy in the calculated longitudinal bending was much more significantly affected by element reduction than the discrepancy in the calculated transverse bending.
- The computational model treating sheets as a single block of material gave significantly larger discrepancies in longitudinal and transverse bending than the computational model using element birth option and taking into account the initial welding gap.

ACKNOWLEDGEMENTS

Financial support of Structural Funds in the Operational Programme - Innovative Economy (IE OP) financed from the European Regional Development Fund - Project "Modern material technologies in aerospace industry", Nr POIG.01.01.02-00-015/08-00 is gratefully acknowledged.

REFERENCES

Adamus, J., Lacki, P., 2014, Analysis of Forming Titanium Welded Blanks, *Comp Mater Sci*, 94, 66-72.

Adamus, K., Kucharczyk, Z., Wojsyk, K., Kudła, K., 2013, Numerical analysis of electron beam welding of different grade titanium sheets, *Comp Mater Sci*, 77, 286-294.

Arai, T., 2010, *The Laser Butt Welding Simulation of the Thin Sheet Metal*, Materials with Complex Behaviour: Modelling, Simulation, Testing and Applications, eds, Öchsner, A., da Silva, L.F.M., Altenbach, H., Springer Verlag, Berlin, 279-296.

Bathe, K.J., 2006, *Finite Element Procedures*, Klaus-Jurgen Bathe.

Deng, D., Murakawa, H., Ma, N., 2012, Predicting Welding Deformation in Thin Plate Panel Structure by Means of Inherent Strain and Interface Element, *Sci Technol Weld Joi*, 17, 13-21.

Koch, F., Enderlein, M., Pietrzyk, M., 2013, Simulation of the Temperature Field and the Microstructure Evolution during Multi-Pass Welding of L485MB Pipeline Steel, *Computer Methods in Material Science*, 13, 173-180.

Lindgren, L.E., 2007, *Computational Welding Mechanics: Thermomechanical and Microstructural Simulation*s, Woodhead Publishing, Abington.

Lacki, P., Adamus, K., Wieczorek, P., 2014, Theoretical and experimental analysis of thermo-mechanical phenomena during electron beam welding process, *Comp Mater Sci*, 94, 17-26.

Matsuoka, S., Okamoto, Y., Okada, A., 2013, Influence of Weld Bead Geometry on Thermal Deformation in Laser Micro-Welding, *Procedia CIRP*, 6, 492-497.

Moein, H., Sattari-Far, I., 2014, Different Finite Element Techniques to Predict Welding Residual Stresses in Aluminum Alloy Plates, *J Mech Sci Technol*, 28, 679-689.

Murakawa, H., Deng, D., Ma, N., Wang, J., 2012, Applications of Inherent Strain and Interface Element to Simulation of Welding Deformation in Thin Plate Structures, *Comp Mater Sci*, 51, 43-52.

Piekarska, W., Kubiak, M., Saternus, Z., 2010, The Model of the Temperature Field and Fluid Flow in Elements Heated by Moving Heat Sources, *Computer Methods in Material Science*, 10, 37-41.

Schenk, T., Richardson, I.M., Kraska, M., Ohnimus, S., 2009, Modeling Buckling Distortion of DP600 Overlap Joints due to Gas Metal Arc Welding and the Influence of the Mesh Density, *Comp Mater Sci*,46, 977-986.

Schultz, H., 2000, *Elektronenstrahlschweißen*, DVS Verlag, Düsseldorf.

Shan, X.Y., Tan M.J., O'Dowd, N.P., 2007, Developing a Realistic FE Analysis Method for the Welding of a NET Single-Bead-on-Plate Test specimen, *J Mater Process Tech*, 192, 497-503.

Słoma, J., Szczygieł, I., Sachajdak, A., 2011, Modelling of Thermal Phenomena in Electric Arc during Surfacing, *Arch Civ Mech Eng*, 11, 437-449.

Sun, J., Liu, X., Tong, Y., Deng, D., 2014, A Comparative Study on Welding Temperature Fields, Residual Stress Distributions and Deformations Induced by Laser Beam Welding and CO^2 Gas Arc Welding, *Mater Design*, 63, 519-530.

Wang, J., Rashed, S., Murakawa, H., Luo, Y., 2013, Numerical Prediction and Mitigation of Out-of Plane Welding Distortion in Ship Panel Structure by Elastic FE Analysis, *Mar Struct*, 34, 135-155.

Winowiecka, J., Więckowski, W., Zawadzki, M., 2013, Evaluation of Drawability of Tailor-Welded Blanks Made of Titanium Alloys Grade 2 || Grade 5, *Comp Mater Sci*, 77, 108-113.

ANALIZA NUMERYCZNA PROCESU SPAWANIA BLACH TYTANOWYCH I ZACHOWANIA SPOINY PODCZAS ROZCIĄGANIA

Streszczenie

W pracy badano zagadnienie spawania blach tytanowych Grade 2 i Grade 5 za pomocą wiązki elektronów. Zespawane blachy stanowią wsad do tłoczenia, w wyniku którego powstaje finalny komponent samolotu.

W procesie spawania wiązka elektronów jest wykorzystywana do stopienia i łączenia materiałów. Spawanie wiązką elektronów charakteryzuje się małą ilością wprowadzanego ciepła, małymi deformacjami, dużą precyzją i powtarzalnością ustawienia parametrów oraz zastosowaniem komory próżniowej. Tytan jest materiałem o wysokim stosunku wytrzymałości do masy, dużej odporności na podwyższone temperatury i środowisko korozyjne. W lotnictwie tytan znajduje zastosowanie w produkcji wirników, silników oraz kadłubów. Tłoczenie wsadów spawanych z różnych materiałów pozwala na uzyskanie komponentów o mieszanych właściwościach składowych materiałów. Tytan Grade 2 zapewnia dobrą tłoczność, natomiast tytan Grade 5 oferuje wysoką wytrzymałość.

Analiza numeryczna procesu spawania koncentrowała się na badaniu wpływu obciążenia termicznego wywołanego przez poruszającą się wiązkę elektronów na deformacje pojawiające się w łączonych blachach. Analizowane blachy miały grubość 0,8 mm. Ich mały przekrój umożliwiał powstawanie znacznych deformacji spawalniczych zarówno w kierunku poprzecznym jak i podłużnym. Jako miarę deformacji przyjęto kąt ugięcia poprzecznego oraz przemieszczenie końca linii spawania. Model numeryczny wykorzystywał Metodę Elementów Skończonych. W symulacji uwzględniono odkształcenia sprężyste, plastyczne oraz termiczne. Do symulacji oddziaływania wiązki elektronów wykorzystano połączone powierzchniowe i objętościowe źródło ciepła. W pracy przedstawiono wpływ struktury siaki elementów skończonych oraz modelu odstępu pomiędzy łączonymi blachami na stopień ugięcia poprzecznego i podłużnego. Uwzględniono siatki o jednorodnej i zmiennej liczbie elementów w kierunku grubości blach i w kierunku linii spawania. Porównano model, w którym blachy stanowiły pojedynczy blok materiału, z modelem, w którym do symulacji odstępu wykorzystano opcję narodzin elementu. Uzyskane wyniki zostały porównane z rzeczywistymi deformacjami zespawanych blach. Analiza procesu spawania została rozszerzona o model opisujący zachowanie próbki wyciętej z połączonych blach podczas statycznej próby rozciągania. Odkształcenia powstające w wyniku rozciągania zostały zmierzone za pomocą systemu optycznego wyposażonego w dwie kamery. Porównano odkształcenia obliczone numerycznie i zmierzone eksperymentalnie.

Received: September 26, 2014
Received in a revised form: November 26, 2014
Accepted: November 29, 2014